

# Mechanics-Based Modeling of Bending and Torsion in Active Cannulas

D. Caleb Rucker, and Robert J. Webster III  
Mechanical Engineering, Vanderbilt University, Nashville, TN 37235

**Abstract**—Active cannulas are meso-scale continuum robots, enabling dexterity in diameters from hundreds of microns to tens of centimeters. Constructed from telescoping, concentric, precurved, superelastic tubes, they exhibit “snake-like” dexterity with a form factor similar to a needle, making them well-suited for applications in minimally invasive surgery. Such applications are facilitated by an accurate kinematic model. The accuracy of prior models has been limited by the assumption of infinite torsional rigidity beyond initial straight transmissions. In this paper, we consider both bending and torsion, describing the total elastic energy stored in two curved concentric tubes. We apply relevant constraints to reduce the energy integral to a classical variational form, in terms of a single unknown function relating tube torsion angles. We then determine the function that minimizes the stored energy analytically, which yields the shape of the active cannula. Experiments demonstrate that this framework can be used predict the shape of a 3-link active cannula more accurately than previous models, reducing tip error by 72% over a bending-only model, and 35% over a model that includes only transmissional torsional. An implication of our work is that the general shape of an active cannula not piecewise constant curvature (as basic assumptions of previous models have implied), but that under certain conditions it may approximate piecewise constant curvature.

## I. INTRODUCTION

The active cannula (Figure 1) is a thin continuum robot design that has the potential to access surgical sites deep within the body through challenging, winding entry trajectories. An active cannula consists of a single “backbone” made from concentric precurved tubes. It bends and changes shape as the tubes translate and rotate axially within one another. This use of elastic tube interaction to achieve bending means that active cannulas do not require support disks or tendon wires [1], [2], flexible push rods [3], pneumatic actuators [4], [5], or other mechanisms external to the central support structure to transmit bending moments. Thus, active cannulas can be small in diameter and have many bending sections. However, the active cannula design also implies that the shape of the individual curved sections are coupled, so that their curvatures cannot (in general) be independently controlled. Still, suitable models can be used to predict and eventually control overall device shape as a function of input degrees of freedom. Design features include miniaturizability, straightforwardness of adding curved sections, and dexterity enhancement with miniaturization [6].

The dexterity and small diameter of active cannulas appear useful in many applications. Among them are a variety of minimally invasive surgical procedures [6], [7], [8], [9], [10] – see [11] for an overview. Perhaps the most promising of

these is access to the lung via the throat. An accurate kinematic model predicting cannula shape as a function of joint variables (axial rotations and translations of the component tubes) is necessary for nearly all potential applications.

The simplest kinematic models of concentric-tube devices similar to active cannulas do not consider either bending or torsion, treating each outer tubes as infinitely rigid compared to all those within it [8]. A substantial improvement in accuracy can be obtained using Bernoulli-Euler beam mechanics to model tube bending [9], [10]. A further enhancement is adding torsional effects in the straight (but not curved) sections of the device [7], [6], and a recent discovery is the fact that end point position (as well as the entire shape) of an active cannula can strongly depend on such torsional effects [6]. In [6] by fitting model parameters to experimental data, an average tip accuracy of 3.0 mm was achieved. However, the difference between predicted and experimental tip positions was not uniform over the workspace, and was worse (8.76 mm) at its edge, where torsional effects are most significant. Additionally, parameters fit to minimize the average tip error were outside their confidence intervals. Both of these facts indicate that it is important to account for torsion more generally - in both curved and straight sections of the cannula, which is the motivation for our current work.

In this paper we proceed by describing the elastic energy stored in an active cannula. We then apply relevant physical considerations and static equilibrium constraints to reduce the energy integral to a variational calculus problem with one unknown function. Application of the Euler-Lagrange equation then yields an extremum (a function that minimizes stored energy). This function fully defines active cannula shape, which we compare with previous bending-only and transmissional torsion models via a set of experiments.



Fig. 1. A prototype active cannula made of superelastic nitinol tubes. Four tubes are shown in the figure above, ranging in diameter from 1.8 mm to 0.5 mm which can rotate and translate with respect to each other to change the cannula’s shape.

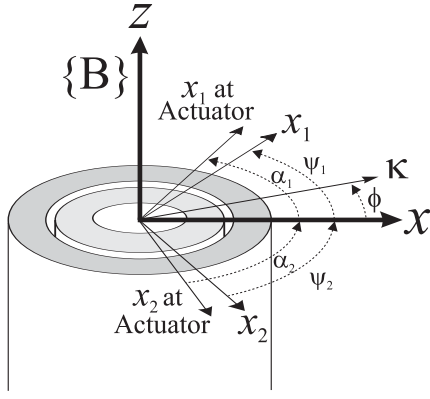


Fig. 2. Cross section of a two tube cannula, showing the relationship between the tube frames and the backbone reference frame  $B$  which is a copy of the world frame “slid” along the backbone, without rotation about the  $z$  axis. The angle  $\phi$  denotes the direction of the resultant curvature vector,  $\kappa$ , for the collection of tubes.

## II. BEAM MECHANICS MODEL WITH TORSION

When a collection of precurved elastic tubes are placed coaxially, they will cause each other to bend. As described in Section I, the resultant shape of the combined tubes has been described by beam mechanics and minimum energy principles [6]. Here, we extend this basic modeling approach to account for torsion in curved sections of the device.

Consider a collection of  $n$  coaxial curved tubes with a world coordinate frame affixed to their collective base, and oriented such that the  $z$  axis is tangent to the tubes. Also consider a collection of  $n$  individual tube reference frames, also with tangent  $z$  axes. These tube frames are functions of arc length ( $s$ ) and thus exist along the backbone. An arbitrary cross section of the backbone is shown in Figure 2. The tube frames rotate with the material as it deforms, keeping track of the current direction of each tube’s precurvature as the tubes undergo bending strain, (rotation about their  $x$  and  $y$  axes), and torsional strain (rotation about their  $z$  axes with respect to the backbone frame  $B$  as shown in Fig. 2). We can describe the final shape of each tube in the tube’s frame with two predefined functions (precurvatures) and three parameters that are functions of arc length.

$$\begin{aligned}
 k_{ix}(s) + \Delta k_{ix}(s) &: \text{Final curvature around the } x\text{-axis of frame } i, \\
 k_{iy}(s) + \Delta k_{iy}(s) &: \text{Final curvature around the } y\text{-axis of frame } i, \\
 \psi_i(s) &: \text{Final rotation of frame } i \text{ around its } z\text{-axis} \\
 &\text{measured with respect to } B
 \end{aligned} \tag{1}$$

where  $k_{ix}$  and  $k_{iy}$  are the the predefined precurvature functions of the  $i^{\text{th}}$  tube in the  $x$  and  $y$  directions, and  $\Delta k_{iy}$  and  $\Delta k_{iz}$  are the changes in curvature caused by interaction with the other  $n - 1$  tubes.

The total energy for the active cannula can then be written [12],

$$U = \frac{1}{2} \int_0^L \left( \sum_{i=1}^n \mathbf{v}_i(s)^T \mathbf{K}_i(s) \mathbf{v}_i(s) \right) ds, \tag{2}$$

where  $L$  is the length of the Cannula,  $\mathbf{v}_i(s) =$

$[\Delta k_{ix}(s) \quad \Delta k_{iy}(s) \quad \psi'_i(s)]^T$ , and the stiffness matrix  $\mathbf{K}_i$  is a diagonal matrix containing tube flexural and torsional stiffnesses, namely  $\mathbf{K}_i(s) = \text{diag}\{E_{ix}(s)I_{ix}(s), E_{iy}(s)I_{iy}(s), G_i(s)J_i(s)\}$ . In the stiffness matrix,  $E$  denotes Young’s Modulus,  $I$  is the cross sectional inertia,  $G$  is the shear modulus, and  $J$  is the polar moment of inertia.

We note that this general parametrization could be used to account for arbitrary precurvature functions for individual tubes, as well as moments of inertia that vary along the length of the tubes. The cannula shape can be determined by finding the functions  $\mathbf{v}_i(s)$  for  $i = 1, \dots, n$  which minimize Equation 2. Clearly this is a challenging task in the general case of Equation 2. However, with appropriate simplifications that account for how active cannulas have been physically constructed to date, the problem becomes more tractable and even analytically approachable via variational calculus in the 2-tube case.

### A. Simplifications from Physical Considerations

For the remainder of this paper we consider a two-tube frictionless cannula where each tube has a constant annular cross section, a straight initial transmission section that leads to a circular arc, and is made of Nitinol. In this case, the initial curvature functions are piecewise constant, and since the tubes are annular and made of a uniform material,  $E, G, I$ , and  $J$  are constants and  $I_y(s) = I_x(s) = I$ . As described in [6] when two tubes of this kind are inserted within one another, there will be four distinct regions or “links” to consider in the overall cannula shape, which begin and end at points where tubes begin and end, or where tubes transition from straight to curved. For example, beginning at the base of the cannula, the links will often be as follows: (1) a link where both tubes are straight, (2) a link where one tube is curved and the other is straight, (3) a link where both tubes are curved, and (4) a link where only one tube is present and curved.

We will begin by examining a link with two curved tubes in isolation, and then incorporate the other links (which are special cases of the two curved tube derivation) to form a complete active cannula model.

For a link as described above, with two curved tubes, we can rewrite Equation 2 as,

$$\begin{aligned}
 U = \frac{1}{2} \int_0^L & E_1 I_1 \Delta \mathbf{k}_1^T \Delta \mathbf{k}_1 + E_2 I_2 \Delta \mathbf{k}_2^T \Delta \mathbf{k}_2 \\
 & + G_1 J_1 \psi_1'^2 + G_2 J_2 \psi_2'^2 \quad ds.
 \end{aligned} \tag{3}$$

where  $\Delta \mathbf{k}_i = [\Delta k_{ix}(s) \quad \Delta k_{iy}(s)]^T$ , and  $L$  is now the total length of the overlapped curves. Our goal is now to find the functions  $\Delta \mathbf{k}_1(s)$ ,  $\Delta \mathbf{k}_2(s)$ ,  $\psi_1(s)$ , and  $\psi_2(s)$  such that  $U$  is locally minimized and initial conditions (tube angles) are satisfied.

### B. Constraint Application

There are several static constraints on the functions in Equation 3 that we can apply to simplify the energy expression further. First, however, we reduce the problem by re-

parameterizing the energy equation as the difference between the tube angles, namely

$$\theta(s) = \psi_2 - \psi_1. \quad (4)$$

One constraint available is a curvature constraint. We assume tubes are fit with close tolerances, such that their tangent vectors will align along their length. Thus tube curvatures (expressed in the same frame) will be equal. Equating them in the frame of tube 1, we can write,

$$\mathbf{k}_1 + \Delta\mathbf{k}_1 = \mathbf{R}_z(\theta)(\mathbf{k}_2 + \Delta\mathbf{k}_2), \quad (5)$$

where  $\mathbf{k}_i = [k_{ix}(s) \ k_{iy}(s)]^T$ , and

$$\mathbf{R}_z(\theta) = \begin{bmatrix} \cos \theta & -\sin \theta \\ \sin \theta & \cos \theta \end{bmatrix}.$$

Another constraint arises from a moment balance. Summing moments about the  $x$  and  $y$  axes in the frame of tube 1 and setting the result equal to zero, we have

$$E_1 I_1 \Delta\mathbf{k}_1 + E_2 I_2 \mathbf{R}_z(\theta) \Delta\mathbf{k}_2 = 0. \quad (6)$$

Solving (5) and (6) simultaneously,

$$\begin{aligned} \Delta\mathbf{k}_1 &= \frac{E_2 I_2}{E_1 I_1 + E_2 I_2} (\mathbf{R}_z(\theta) \mathbf{k}_2 - \mathbf{k}_1), \\ \Delta\mathbf{k}_2 &= \frac{E_1 I_1}{E_1 I_1 + E_2 I_2} (\mathbf{R}_z(\theta)^T \mathbf{k}_1 - \mathbf{k}_2). \end{aligned} \quad (7)$$

Since both tubes have circular precurvature we can, without loss of generality, attach their individual tube frames such that the  $x$  axis of the tube frame is perpendicular to the plane of the arc. This implies that the precurvature will be completely in  $x$  and zero in  $y$ . Thus, for the remainder of the derivation, we will drop the  $x$  subscript from  $k_{1x}$  and  $k_{2x}$  in favor of  $k_1$  and  $k_2$ .

One more constraint is available from a moment balance about the  $z$  axis. Summing moments in the frame of tube 1 and setting the result equal to zero, we have

$$G_1 J_1 \psi_1' + G_2 J_2 \psi_2' = 0. \quad (8)$$

Taking the derivative of both sides of Equation 4 with respect to  $s$  and solving simultaneously with Equation 8 yields

$$\psi_1' = -\frac{G_2 J_2}{G_1 J_1 + G_2 J_2} \theta', \quad \text{and} \quad \psi_2' = \frac{G_1 J_1}{G_1 J_1 + G_2 J_2} \theta'. \quad (9)$$

Thus, Equation 3 can be written in terms of one unknown function ( $\theta(s)$ ) as follows,

$$\begin{aligned} U &= \frac{1}{2} \int_0^L \frac{E_1 I_1 E_2 I_2}{E_1 I_1 + E_2 I_2} (k_1^2 + k_2^2 - 2k_1 k_2 \cos \theta) \\ &\quad + \frac{G_1 J_1 G_2 J_2}{G_1 J_1 + G_2 J_2} \theta^2 \ ds. \end{aligned} \quad (10)$$

To understand the shape of links in which at least one tube is straight, consider Equation 10 when one or both  $k_i$  are zero. In this case, the first term does not depend on  $\theta$ , meaning it is simply a constant and plays no role in the minimization of energy. Based on this it is easy to see that even if one tube is curved, the pair of tubes will behave as

they will in the section where both both tubes are straight, with respect to  $\theta$ . That is  $\theta$  will vary linearly along the link.

Now that we have formulated the energy of the active cannula in terms of one unknown function, we can apply tools from variational calculus to analytically determine the minimizing function, which is the topic of the following section.

### III. VARIATIONAL SOLUTION

Equation 10 has the classic variational calculus form,

$$U = \int_0^L f(s, \theta(s), \theta'(s)) ds, \quad (11)$$

where the goal is to find  $\theta(s) \in \{C^1[0, L], \theta(0) = \theta_0, \theta'(L) = 0\}$  such that  $U$  is minimized. We can derive a differential equation defining  $\theta(s)$  by realizing that any function which minimizes Equation 10 must satisfy the Euler-Lagrange differential equation,

$$0 = \frac{\partial E}{\partial \theta} = \frac{\partial f}{\partial \theta} - \frac{d}{ds} \left( \frac{\partial f}{\partial \theta'} \right), \quad (12)$$

where  $f$  is the integrand of Equation 10. Applying the Euler-Lagrange equation to  $f$  we obtain

$$\theta'' - \frac{A}{2} \sin \theta = 0 \quad (13)$$

where  $A$  is a constant given by

$$A = 2k_1 k_2 \frac{E_1 I_1 E_2 I_2 (G_1 J_1 + G_2 J_2)}{G_1 J_1 G_2 J_2 (E_1 I_1 + E_2 I_2)}. \quad (14)$$

As mentioned above, our boundary conditions are  $\theta(0) = \theta_0$  and  $\theta'(L) = 0$ .

Note that Equation 13 has the same form as the differential equation which governs the motion of a simple inverted pendulum. Thus, we can think of  $\theta(s)$  changing along the backbone of the tubes in the same way that the angle of an inverted pendulum changes through time. At first this seems counter-intuitive, since we do not expect  $\theta$  to oscillate. However, Equation 13 only describes the cannula for  $s \in [0, L]$ . Thus, analogy makes sense if one considers an inverted pendulum with an initial angle  $\theta_0$  and an initial angular velocity  $\theta_0'$  upward. In the analogy, the ‘‘pendulum’’ swings toward zero (vertical) while slowing down until its velocity reaches zero. Then, instead of falling back downward, the tubes end which corresponds to time ending in the pendulum analogy.

We can solve Equation 13 analytically in a similar manner to the pendulum equation. Multiplying both sides by  $\frac{d\theta}{ds}$ , integrating, and applying the boundary condition  $\theta_L' = 0$ , we get

$$\theta'^2(s) + A \cos \theta(s) = A \cos \theta_L. \quad (15)$$

Rearranging (15) and integrating again, we obtain

$$s = \pm \frac{1}{\sqrt{A}} \int_{\theta_0}^{\theta(s)} \frac{d\theta}{\sqrt{\cos \theta_L - \cos \theta}} \quad (16)$$

This integral equation defines  $\theta(s)$ , and it is possible to write  $\theta(s)$  as a combination of elliptic integrals of the first kind as follows.

Using  $\cos(\theta + \pi(1 + 2k)) = -\cos \theta \quad \forall k \in \mathbf{Z}$ , recognizing that  $\cos 2\theta = 1 - 2\sin^2 \theta$ , and letting  $\gamma = \frac{\theta + \pi(1 + 2k)}{2}$  we can write

$$s = \pm \sqrt{\frac{2m}{A}} \int_{\gamma(0)}^{\gamma(s)} \frac{d\theta}{\sqrt{1 - m\sin^2(\gamma)}} \quad (17)$$

$$\Rightarrow s = \pm \sqrt{\frac{2m}{A}} \left( F(\gamma(s), m) - F(\gamma(0), m) \right)$$

where

$$m = \csc^2 \gamma_L = \frac{2}{1 + \cos \theta_L} = \frac{2A}{A + \theta_0'^2 + A \cos \theta_0}, \quad (18)$$

and  $F(\gamma, m)$  is the elliptic integral of the first kind with amplitude  $\gamma$  and modulus  $m$ . We can now use the Jacobi Amplitude function,  $am$ , which is the inverse function of  $F$  defined by the identity

$$am(F(\gamma, m), m) = \gamma \quad (19)$$

to obtain the following solutions

$$\theta(s) = 2am \left( F(\gamma(0), m) \pm \sqrt{\frac{A}{2m}} s, m \right) - \pi(1 + 2k) \quad (20)$$

$$\theta'(s) = \pm \sqrt{\frac{2A}{m}} dn \left( F(\gamma(0), m) \pm \sqrt{\frac{A}{2m}} s, m \right)$$

where  $dn$  is a Jacobi elliptic function defined as

$$dn(u, m) = \sqrt{1 - m\sin^2 am(u, m)}. \quad (21)$$

We must note here that  $m \geq 1$  by definition, while the classic definitions the elliptic integral and Jacobi functions limit  $m$  to the range  $0 \leq m \leq 1$ . If  $m \geq 1$ , then the Jacobi Amplitude function is periodic, and (19) only holds for  $-\pi/2 \leq \gamma \leq \pi/2$ . The peak to peak amplitude of  $am$  is no more than  $\pi$  for  $m \geq 1$ , so  $|\theta(0) - \theta(s)| \leq 2\pi$  and we can choose  $k = \lfloor -\theta/2\pi \rfloor$  so that (19) always applies. In [6] torsion is considered in straight transmission sections of a cannula. It was shown that in this case, multiple solutions (local minimum energy configurations) can emerge. We see the same phenomenon here. Equation 20 contains the unknown boundary condition  $\theta_0'$  within  $m$ . In general, there may be more than one value for  $\theta_0'$  which can be chosen so that the solution satisfies the boundary condition  $\theta_L' = 0$ . We can use numerical root finding techniques to search for solutions and choose the one which corresponds to the observed configuration. The  $\pm$  signs in (20) take the same sign as the chosen value for  $\theta_0'$ .

As noted in [6] the particular local minimum energy configuration in which the system rests will be path dependent. For example, if one has reached the current set of actuator inputs by rotating a tube in the positive direction, one solution will be indicated, whereas getting to the same actuator state by rotating the opposite way will result in a different solution. In general, the system will stay in the same energy minimum until it disappears, leaving a continuously decreasing energy path to a new minimum.

### A. Generalizing to Three Links

The results from the analysis of one link presented in previous sections can be used to solve for the shape of a multi-link cannula described in Section II. We will keep the transition point where both tubes become curved as our arc length zero ( $s = 0$ ) so that we can use the equations derived above unaltered. Using the fact that  $\theta$  varies linearly with arc length in the sections which have at least one straight tube and the fact that the moments about the  $z$  axes to achieve  $\alpha_1$  and  $\alpha_2$  must balance, we obtain the following relationship:

$$\theta_0' = (\theta_0 - \alpha_1 + \alpha_2) \frac{G_1 J_1 + G_2 J_2}{G_1 J_1 D_2 + G_2 J_2 D_1} \quad (22)$$

Where  $D_1$  and  $D_2$  are the arc lengths between the actuators and the link in which both tubes are curved. By substituting this onto (15), we now have  $m$  and thus (20) in terms of  $\theta_0$ . We then use Mathematica's `RootFind` function to solve for a value of  $\theta_0$  for which  $\theta_L' = 0$ .

Once  $\theta_0$  is known, the function  $\theta(s)$  is fully defined. It changes linearly from its initial value to  $\theta_0$ , then is and then is defined along the link where both tubes are curved by Equation 20. In the final link, only one tube is present, so the curvature of this link is simply the precurvature of the single tube, and the plane of the link is the same as  $\psi$  for that tube at the end of the previous link. From here it is straightforward to obtain  $\psi_1$ , and  $\Delta \mathbf{k}_1$ , using the relationships given in Section II and the actuator inputs. We can then transform the final curvature of either of the tubes ( $\mathbf{k}_i + \Delta \mathbf{k}_i$ ), into the backbone reference frame  $B$ , approximate it with many small piecewise constant segments, and apply the product of exponentials formula [6] which will yield the overall shape of the active cannula.

## IV. EXPERIMENTAL RESULTS AND DISCUSSION

In [6], experimental shape data for a two tube cannula was gathered and compared to theoretical predictions. The model used for those predictions considered torsion only in initial straight transmissions between actuators and curved sections of the cannula, as discussed in Section I. In this section, we will compare the predictions of the model given in [6] with the more general model given in Section II. The experimental data set used is the same as that presented in [6].

In the experiments, an outer tube and an inner wire were arranged in two different translational positions and a range of input angles was applied at each. The resultant overall

	Outer Tube	Inner Wire
Poisson's Ratio	4.25	4.25
Young's Modulus (MPa)	58	58
Inner Diameter (mm)	2.01	0
Outer Diameter (mm)	2.39	1.60
Straight Length (mm)	93.5	218.5
Curved Length (mm)	92.3	85
Curvature (1/mm)	0.0099	0.0138

TABLE I  
MEASURED AND ASSUMED PHYSICAL QUANTITIES  
FOR EXPERIMENTAL TUBE AND WIRE.

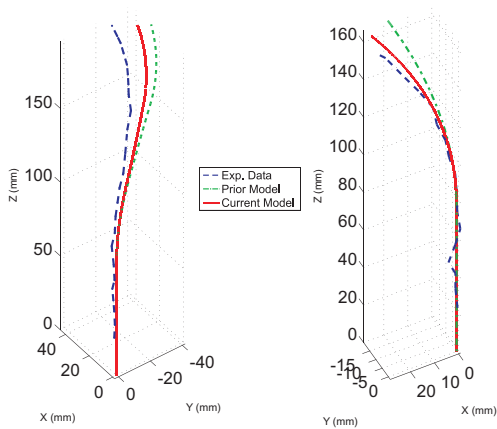


Fig. 3. Comparison of shape for the model of [6] (green), the model given in Section II (red) and experimental data (blue) for configurations near the edge of the active cannula workspace. Note that the model given in Section II produces predictions closer to experimentally observed cannula shape. Left: partial overlap case, Right: full overlap case. Units are mm.

shape of the cannula was recorded in each experiment via stereo imaging with fiducial markers as described in [6]. In [6] model parameters were then fit to the experimental data, to minimize the average error in tip prediction. In the context of the general torsional model that is the focus of our current work, such a fitting process is left to future work. Here we use “nominal properties” – those that would be read from a data sheet or looked up on tables. These properties are summarized in Table I. A complete discussion of parameter ranges, uncertainties, nominal parameters, and parameter fitting can be found in [11]. The physical quantities listed on the table were used in both the model of [6] and the general torsional model derived in this paper, so that the models could be directly compared in terms of predictive ability without fitting.

To summarize the experimental dataset of [6], the two translational positions were referred to as the “full overlap case” and the “partial overlap case”. In the full overlap case, the tube and wire were arranged so that the link lengths were:  $l_1 = 10\text{mm}$  (tube curved, wire straight),  $l_2 = 82.3\text{mm}$  (both curved), and  $l_3 = 2.7\text{mm}$  (only wire present). For the full overlap case, data were recorded for 15 different input angles ranging from  $0^\circ$  to  $280^\circ$  in  $20^\circ$  increments. In the partial overlap case, the tube and wire were arranged so that the link lengths were:  $l_1 = 48\text{mm}$ ,  $l_2 = 44.3\text{mm}$ , and  $l_3 = 40.7\text{mm}$ . For this overlap configuration, data were recorded for 11 different input angles ranging from  $0^\circ$  to  $200^\circ$  in  $20^\circ$  increments.

Plots of the experimental cannula shape data are shown in Figure 3 together with the predictions of the two models for the two cases. Pictured are the “worst-cases” – the angular input angles at the edge of the workspace, where torsion is most significant. These are  $280^\circ$  in the full overlap case, and  $200^\circ$  in the partial overlap case. The behavior pictured is typical of all experimental positions, namely that the prediction of the model derived in Section II lies nearer the

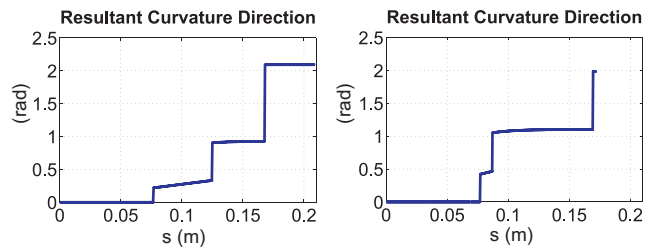


Fig. 4. Angle  $\phi$  of the resultant curvature vector ( $\kappa$  in Figure 2), that defines the instantaneous plane of curvature of the active cannula. Left: partial overlap case, Right: full overlap case.

experimental data than the transmissional torsional model in [6]. The model of Section II has an average tip error of 6.50 mm across all experiments, compared to 10.0 mm for the transmissional torsion model of [6], and 23.2 mm for a model that assumes infinite torsional rigidity (also described in [6]). We note that with parameter fitting, the average tip error was reduced to 3.0 mm in [6], and it is reasonable to expect a similar reduction with the model of Section II, which is a topic of future investigation.

The model of Section II also allows us to investigate a modeling assumption that has been common to all prior work, that tubes with circular precurvature will produce a circular resultant shape when placed within one another and rotated axially. With the model of Section II we obtain equations for cannula curvature in the  $x$  and  $y$  directions of the reference frame. The resultant curvature vector of these components makes an angle  $\phi$  about the  $z$  axis, measured with respect to the  $x$  axis of  $B$ , as shown in Figure 2. If the resultant shape of the concentric tubes were circular,  $\phi$  should be constant. Plotting  $\phi$  for our model of the experimental cannula (Figure 4) shows that while  $\phi$  is not exactly piecewise constant, it is approximately so. This illustrates why previous studies (e.g. [7], [10]) have included the modeling assumption of no torsional strain in the curved sections, which implies piecewise constant curvature. The out of plane motion was small enough that it was not obvious experimentally.

However, it is instructive to simulate a cannula with longer arc length. In Figure 5 we simulate two tubes with the same cross sections, material properties, and curvatures as the tubes used in our experiments described above. Here we simulate an initial straight length of zero, and a curved length of  $636\text{mm}$  for both tubes. This arc length corresponds to one full circle for the outer tube. The input angle difference between the tubes is set to  $350^\circ$ . It is clear from Figure 5 that the resulting shape does not lie in a plane even though the precurvature of each tube is a planar circular arc. This is further illustrated by an examination of  $\phi$  with respect to arc length, as shown in Figure 6. These experimental and simulation results explain why the circular assumption has been a good one for the prototype cannulas that have been constructed to date, which have arc lengths much less than a full circle. It also indicates that if longer cannulas are desired (or other parameters are varied), a more general model, such

as the one presented in this paper will likely be required.

## V. CONCLUSIONS AND FUTURE WORK

The general modeling framework proposed in this paper is a step toward a comprehensive model for both bending and torsion throughout an active cannula, which promises substantial improvements in predictive power. It is clear that the energy functionals derived in this work are generalizable to  $n$  tube cannulas, as well as arbitrary input precurvature functions and variable stiffness along the tubes. It also appears feasible in future work to generalize our variational approach, converting such functionals into sets of differential equations. While it may be challenging to derive analytical solutions to these sets of differential equations, efficient numerical solutions will likely be possible.

The purpose of the experiments described in this paper was comparison between our new model and prior models, and the substantial accuracy improvements indicate that the model is not over-fitting the data. In future work we intend to probe the limits of the accuracy of our new modeling framework through further experiments as well as apply parameter identification procedures similar to those in [6]. The ultimate goal of such modeling efforts is a kinematic model that will be accurate enough for all possible surgical and non-surgical applications, including microsurgery with very small active cannulas. These models will form the basis for closed-loop cannula control, and will facilitate the design of patient-specific cannula tube shapes. Such advancements are likely to profoundly improve the dexterity of robots,

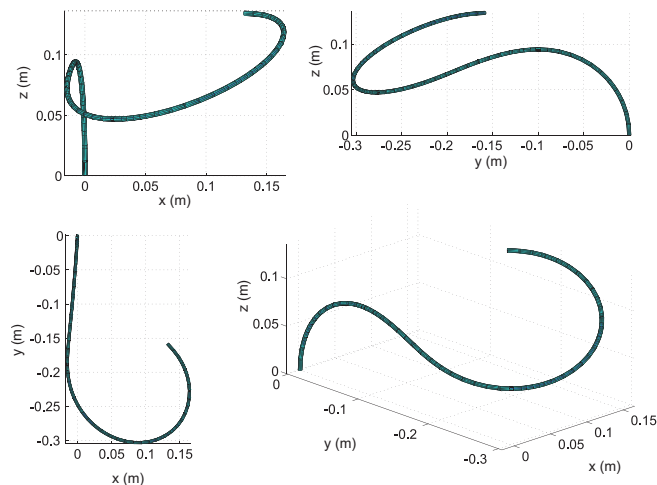


Fig. 5. Shown above are four projections of a simulation of two fully precurved, fully overlapping tubes, whose material properties and curvatures match our experimental cannula. Units are m. The difference between the experimental cannula and the simulation are longer arc length (equal to one full circle of the outer tube) and an input angular difference of  $350^\circ$  at the tube bases. It is evident from this simulation that tubes with circular precurvature do not combine to form a circular resultant shape under all conditions.

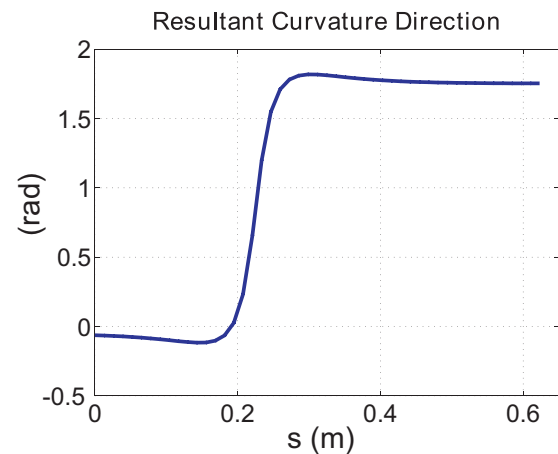


Fig. 6. Angle  $\phi$  as a function of arc length for the simulation shown in Figure 5.

leading to substantial advancements in human ability to treat disease with minimal trauma to healthy tissues.

## VI. ACKNOWLEDGEMENTS

This work was supported by National Science Foundation through CBET 0651803, and an NSF graduate fellowship.

## REFERENCES

- [1] M. W. Hannan and I. D. Walker, "Kinematics and the implementation of an elephant's trunk manipulator and other continuum style robots," *Journal of Robotic Systems*, vol. 20, no. 2, pp. 45–63, 2003.
- [2] P. Dario, M. C. Carrozza, M. Marcacci, S. D'Attanasio, B. Magnani, and G. M. O. Tonet, "A novel mechatronic tool for computer-assisted arthroscopy," *IEEE Transactions on Information Technology in Biomedicine*, vol. 4, no. 1, pp. 15–29, 2000.
- [3] N. Simaan, R. Taylor, and P. Flint, "A dexterous system for laryngeal surgery," *IEEE International Conference on Robotics and Automation*, pp. 351–357, 2004.
- [4] G. S. Chirikjian, "Kinematic synthesis of mechanisms and robotic manipulators with binary actuators," *Journal of Mechanical Design*, vol. 117, pp. 573–580, 1995.
- [5] B. A. Jones, W. McMahan, and I. D. Walker, "Practical kinematics for real-time implementation of continuum robots," *IEEE International Conference on Robotics and Automation*, pp. 1840–1847, 2006.
- [6] R. J. Webster III, J. M. Romano, and N. J. Cowan, "Mechanics of precurved-tube continuum robots," *IEEE Transactions on Robotics*, 2008, (Accepted).
- [7] R. J. Webster III, A. M. Okamura, and N. J. Cowan, "Toward active cannulas: Miniature snake-like surgical robots," *IEEE/RSJ International Conference on Intelligent Robots and Systems*, pp. 2857–2863, 2006.
- [8] J. Furusho, T. Katsuragi, T. Kikuchi, T. Suzuki, H. Tanaka, Y. Chiba, and H. Horio, "Curved multi-tube systems for fetal blood sampling and treatments of organs like brain and breast," *Journal of Computer Assisted Radiology and Surgery*, pp. 223–226, 2006.
- [9] M. Loser, "A new robotic system for visually controlled percutaneous interventions under X-ray or CT-fluoroscopy," Master's thesis, The Albert-Ludwig-University, Freiburg, Germany, September 2002.
- [10] P. Sears and P. E. Dupont, "A steerable needle technology using curved concentric tubes," *IEEE/RSJ International Conference on Intelligent Robots and Systems*, pp. 2850–2856, 2006.
- [11] R. J. Webster III, "Design and mechanics of continuum robots for surgery," Mechanical Engineering, Johns Hopkins University, Baltimore, MD, December 2007, PhD Thesis.
- [12] N. J. Cowan, personal communication, 2008.